

Influence of boundary roughness on the magnetization reversal in submicron sized magnetic tunnel junctions

D. Meyners,^{a)} H. Brückl, and G. Reiss

Nano Device Group, Department of Physics, University of Bielefeld, P.O. Box 100131, 33501 Bielefeld, Germany

(Received 30 August 2002; accepted 18 December 2002)

The reproducible magnetic switching of submicron magnetic tunnel junctions (MTJ's) is an important requirement for their application in highly integrated magnetic memory devices. We have investigated the switching of small MTJ's by atomic and magnetic force microscopy (AFM/MFM) combined with micromagnetic numerical simulations. The latter are carried out with the real (AFM) shape as input mask, including the boundary roughness of the MTJ's. MFM reveals S-, C-, and K-shaped magnetization patterns for rectangular submicron sized junctions in saturation. In general, the magnetization loops and switching fields are different for individual junctions. The simulations show that the detailed boundary shape, which is specific for each junction, has a significant influence on the nucleation and location of domain walls and vortices, and hence, on the magnetic switching.

© 2003 American Institute of Physics. [DOI: 10.1063/1.1544424]

I. INTRODUCTION

In recent years, the interest in magnetic tunnel junctions (MTJ's) has increased due to their high potential as memory cells in magnetic random access memories or read heads in hard disk drives.¹⁻³ Nevertheless, the magnetic switching behavior of MTJ's with lateral extensions below 1 μm is not yet understood in detail. Distorted switching curves (astroids) obtained from magnetoresistance curves were reported by, e.g., Klostermann *et al.*⁴ Moreover, identically prepared tunnel junctions show different junction specific switching behavior.^{5,6} On the one hand, the physical origin of these variations is unknown up until now, on the other hand, they limit the technical applicability of the MTJ's.

In this work, we present investigations of sub- μ magnetic tunnel junctions by atomic force microscopy (AFM) and magnetic force microscopy (MFM) in combination with micromagnetic numerical simulations. The lithographic steps in the fabrication process inevitably lead to imperfect rough boundaries of the MTJ's on the nanometer scale. The impact of these structural imperfections on the magnetic switching behavior will be discussed.

II. EXPERIMENT

The preparation of the film stack and the lithographic electron-beam (e-beam) procedure was described in detail elsewhere.⁷ The magnetically hard layer of the tunnel junctions consists of an artificial antiferromagnet CoFe 1.5 nm/Ru 0.9 nm/CoFe 2.2 nm. The 6 nm thick $\text{Ni}_{81}\text{Fe}_{19}$ soft electrode is separated by a 1.5 nm thick Al_2O_3 barrier. Junctions with different shapes and sizes were investigated: Rectangular junctions ranging from 700 nm \times 700 nm to 700 nm \times 1400 nm and elliptical patterns with 500 nm short axes and 850 nm long axes. The patterns were covered by a 15 nm

thick Ta layer which minimizes stray field effects of the MFM tip and, hence, tip induced perturbations of the soft layer magnetization. Furthermore, the magnetic moment of the home made MFM probes was adjusted by varying the thickness of the magnetic coating. A stack of 5 nm Ta/15 nm ... 90 nm CoCr/2 nm Co/5 nm Ta was deposited by sputtering onto commercially available probes for the dynamic AFM mode.⁸ The Ta layers serve both as a seed layer and oxidation protection. The thin Co layer increases the remanent magnetization of the probe without a significant decrease of its anisotropy field.⁹ Sufficient signal-to-noise ratio and small perturbations were obtained for a CoCr thickness of 30 nm.

For the MFM investigations, a modified Nanoscope III from Digital Instruments was operated in the Lift-ModeTM. The magnetic field was generated by two pairs of coils surrounding the microscope. MFM images of the magnetization of the patterned NiFe electrodes were recorded at different external fields.

Figure 1 shows the AFM topography of typical tunnel junctions with rectangularly patterned electrodes of 700 nm \times 700 nm and 700 nm \times 1400 nm sizes. The roughness of the boundary and the round corners are clearly visible. As these imperfections originate from film crystallinity and e-beam resist granularity after exposure, their appearance is statistical and different for each junction. The influence of these irregular boundaries on the magnetization dynamics of the NiFe electrodes can be simulated by the numerical solution of the Landau-Lifshitz equation. For this special task, the junction specific boundaries from AFM measurements are taken as input for the OOMMF program (release1.1) developed at the National Institute for Standards and Technology (Gaithersburg, MD).¹⁰ The calculations, which neglect the magnetically hard layer, are carried out with the following material parameters for $\text{Ni}_{81}\text{Fe}_{19}$: Exchange stiffness $A = 6.5 \times 10^{-12}$ J/m, bulk saturation magnetization $M_S = 860$ kA/m, uniaxial anisotropy constant $K_1 = 270$ J/m³, which was determined from experiment. The uniaxial anisot-

^{a)}Electronic mail: meyners@physik.uni-bielefeld.de

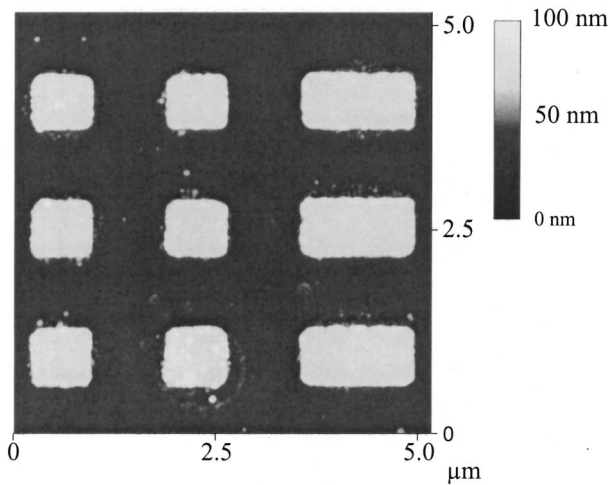


FIG. 1. AFM topography of MTJ's with rectangularly patterned Ni₈₁Fe₁₉ electrodes.

ropy directions are randomly distributed in the calculation cells (cell size=5 nm...6.3 nm). In order to simulate a minor loop, solutions are computed successively for different external magnetic field values, starting with a remanent state and switching on the maximum field used in the simulations. The convergence criterion is $\text{MAX}_i\{|\mathbf{M}_i \times \mathbf{H}_{\text{eff}_i} / M_s^2|\} < 10^{-5}$. \mathbf{M}_i is the magnetization and $\mathbf{H}_{\text{eff}_i}$ the effective field of cell i .

III. RESULTS

A. Micromagnetic numerical simulations: Rectangular junctions

The rectangular electrodes develop S, C, or K states at the beginning of the minor loops (Fig. 2). Small deviations of these basic states arise from roughness and the details of the individual shape. These deviations strongly influence the detailed switching behavior of the junctions, as will be shown in the following.

In junctions with initially S-shaped magnetization, the nucleation and stability of domain walls are significantly influenced by boundary roughness. The calculated minor loops for two junctions with different boundary roughness are compared in Fig. 3. If the boundary roughness is small, the magnetization switches rotation like at magnetic fields smaller than 6 kA/m without nucleation of stable domain walls (crosses in Fig. 3). The central magnetization is re-

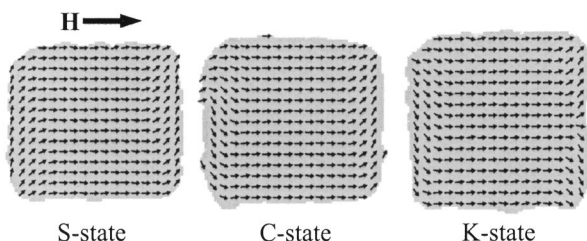


FIG. 2. Typical magnetization configurations near saturation of rectangular junctions. The external magnetic field H is 6 kA/m. The shape of the junctions varies due to lithographic imperfections and is about 700 nm \times 700 nm.

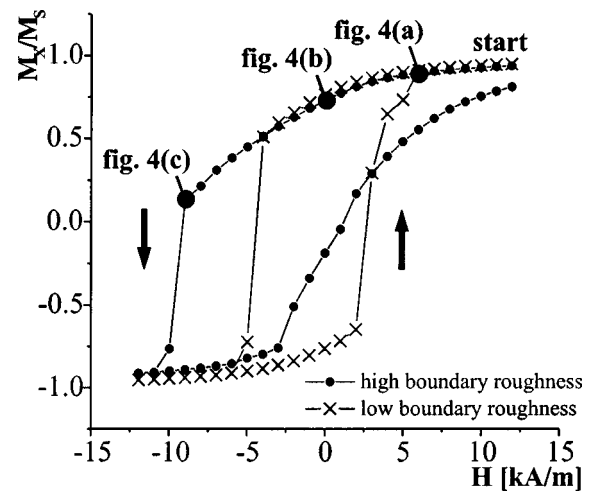


FIG. 3. Minor loops of two rectangularly patterned junctions. M_x/M_s is the magnetization of the NiFe electrodes parallel to the external field H . Both loops start with a S-shaped magnetization at $H = 11.9$ kA/m. Corresponding magnetization configuration for the rough boundary element (circles) are shown in Fig. 4.

versed prior to the magnetization in regions close to the boundary. The size and stability of the resulting edge domains depend obviously on boundary roughness. Their successive annihilation leads to the small steps observed in the minor loop close to saturation. On the other hand, a rough boundary with a 20 nm deep cleft acts as a pinning center for a Néel domain wall. A direct consequence is the increase of the switching field to around -10 kA/m (solid circles in Fig. 3). Wall nucleation and pinning at the cleft is illustrated in Fig. 4: Starting with an S-shaped configuration similar to the MTJ with smooth boundaries, the lateral extension of the edge domains increases with decreasing magnetic field. In order to reduce the stray field, the magnetization aligns nearly parallel to the boundary. At the position of the cleft, this gives rise to a disturbance of the magnetization [Fig. 4(b)]. If the external magnetic field is increased in the opposite direction, the magnetization on the left- and on the right-hand side of the cleft rotates in different directions. This

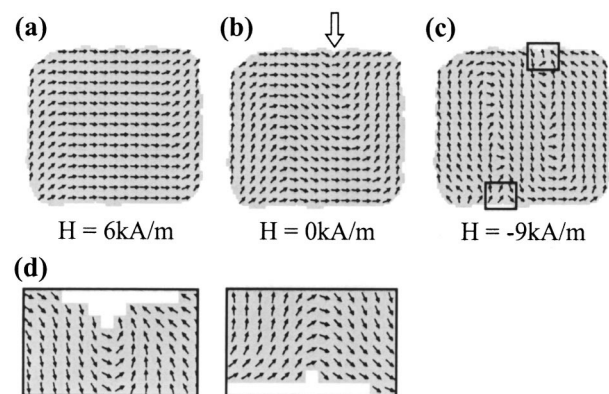


FIG. 4. (a)–(c) Examples of calculated magnetization configurations obtained in the minor loop of Fig. 3 illustrating domain-wall pinning at a 20 nm deep cleft in the upper boundary [thick arrow in (b)]. (d) Magnified view of the marked areas in (c). The positions of the two nucleated Néel domain walls coincide with the location of two clefts in the boundaries.

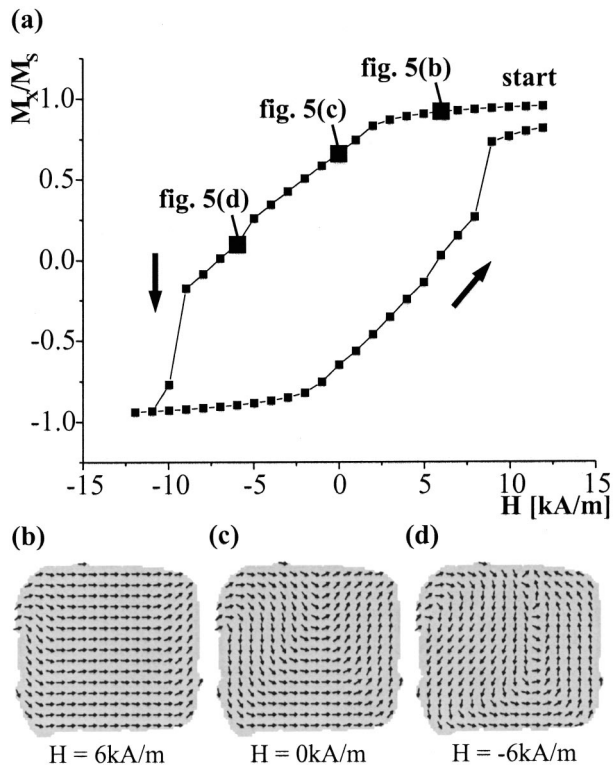


FIG. 5. Wall nucleation from initially C-shaped magnetization (element size: $700\text{ nm} \times 700\text{ nm}$). (a) Magnetization curve. (b)–(d) Typical magnetization configurations.

leads to the nucleation of two 180° Néel walls and switching occurs at a magnetic field of -10 kA/m . During subsequent reduction of the external field, a vortex appears, whose center moves through the electrode leading to nearly zero remanent magnetization and a saturation field larger than 11.9 kA/m (Fig. 3).

As shown, although both junctions start with an S-shaped magnetization configuration, the completely different switching behavior has its origin in their different boundary shapes. Rough boundaries and clefts act as pinning centers which decrease wall mobility and lead to significantly larger switching fields whereas a small roughness can help to nucleate walls and promote switching.¹¹ Zheng *et al.*¹² computed magnetization reversals for rectangularly patterned electrodes and showed that the switching fields of electrodes with initial S states are definitely lower than for electrodes with initial C states. These simulations were carried out for patterns with ideally smooth boundaries. Our calculations show that for junctions with realistic, i.e., rough, boundaries, initially S-shaped magnetization is not sufficient for reasonably small switching fields.

Although the detailed magnetization reversal in a minor loop is strongly influenced by junction specific roughness, some features are common. Junctions with initial C configuration always show the nucleation of stable 180° Néel walls and high switching fields, which is in agreement with Zheng *et al.*¹² Figure 5 shows examples of calculated magnetization patterns and the according magnetization curve of a junction with initial C state, which deviates from the ideal state at the left-hand side upper corner due to the round boundary shape

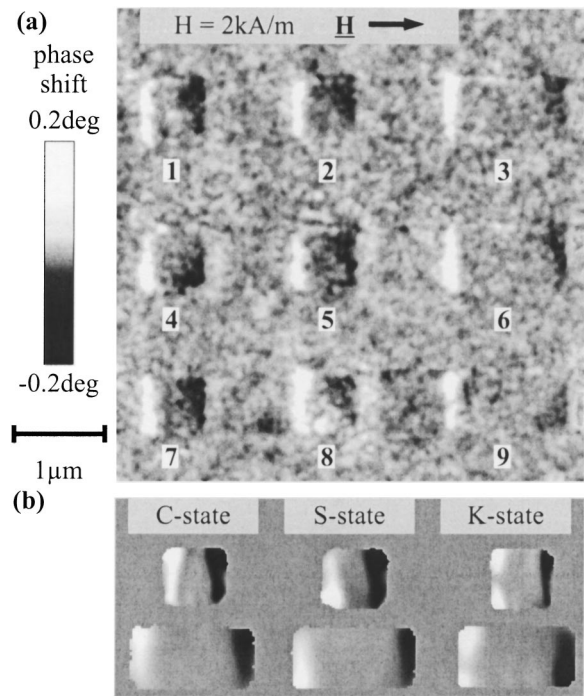


FIG. 6. (a) MFM image of the NiFe electrodes shown in Fig. 1. The external magnetic field is 2 kA/m . The electrodes are marked by numbers for easier reference. (b) Calculated MFM images from magnetization configurations found in the micromagnetic numerical simulations. All experimental MFM images are processed by a lowpass filter.

[Fig. 5(b)]. After sign reversal of the external magnetic field, a stable wall is generated [Figs. 5(c) and 5(d)]. The deviation from a perfect rectangle and the related ideal C state causes their asymmetric location with respect to the center. This wall leads to a large switching field of about -10 kA/m [Fig. 5(a)]. The total loop, again, is not symmetric and has two different switching fields.

B. Domain observation by magnetic force microscopy: Rectangular junctions

Figure 6 shows a MFM image of the rectangular electrodes of Fig. 1 at a field of 2 kA/m and, for comparison, simulated MFM images calculated using the magnetization configurations given by the micromagnetic simulations. In this calculation, the point probe is scanned in a height of 100 nm to 125 nm , which is twice the real tip scanning height, because the position should be chosen in the center of the magnetically active volume of the MFM probe.¹³

All junctions in Fig. 6(a) show edge contrast with varying lateral extension of 140 nm to 350 nm . The contrast between the electrodes is mainly due to thermal noise, although a partial contribution from the buried artificial anti-ferromagnet cannot be excluded. Its magnetic behavior was reported in detail elsewhere.¹⁴ By comparison with the calculated images in Fig. 6(b) C, S, and K states can be attributed to the junctions, i.e., C state to 3 and 4, S state to 6 and 7, and K state to 9.

The further development is illustrated in Fig. 7. The MFM image was taken at an external field of -1.5 kA/m [Fig. 7(a)]. Junctions 6 and 9 show configurations, which are

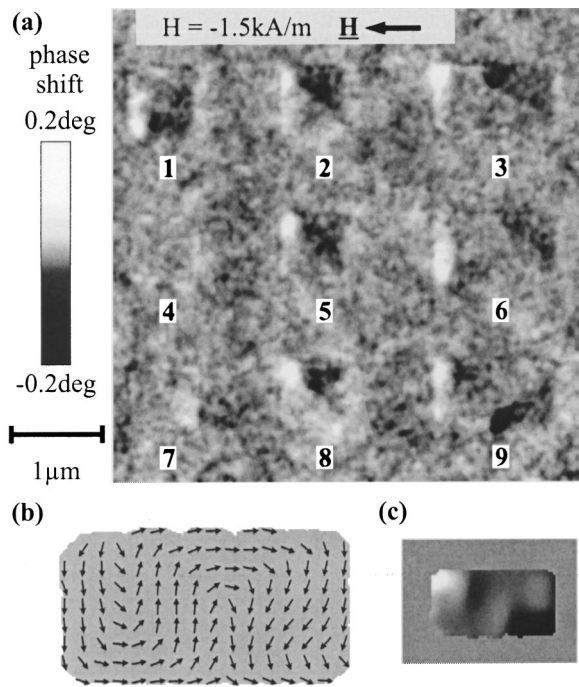


FIG. 7. (a) MFM image of the rectangular NiFe electrodes of Fig. 1 illustrating a further stage of the magnetization loop. (b) Calculated magnetization configuration: The reversed external field leads to a rotation of the magnetization in the edge domains of the electrodes with aspect ratio 1:2. (c) The calculated MFM contrast from (b).

reproduced by the micromagnetic simulations [Fig. 7(b)]. The external magnetic field causes a rotation of the magnetization in the edge domains. This leads to the nucleation of 180° Néel walls giving the typical light and dark contrast in the MFM image. There is a good correspondence between the experimental and the calculated MFM image [Fig. 7(c)]. Because electrode 9 started with a K-shaped magnetization, there is an additional bright contrast in the lower left-hand side corner of the junction due to an additional small edge domain.

Usually, at identical junctions, the results of the micromagnetic simulations do not quantitatively agree with the MFM images. There are at least two reasons for this deviation. First, the influence and the stray field of the artificial antiferromagnet is neglected in the calculations due to limitations of the OOMMF program. Second, despite of the random local fluctuations of the crystalline anisotropy in the NiFe layer, there is a possibility of a preferential uniaxial anisotropy direction in the electrodes due to the preparation by magnetron sputtering, which is not correctly described by the random distribution in the calculation.

The magnetic contrast of the electrodes 4 and 7 changes and nearly disappears during imaging [Fig. 7(a)]. These electrodes were macroscopically switched by the stray field of the probe. Such perturbations appear, if the magnetization configurations are close to switching, i.e., sensitive to small changes in the external magnetic field. We thus can use this effect for an additional characterization by defining the field, where the tip-sample interaction starts to perturb the imaging as onset field H_{on} . As shown in Table I, H_{on} is junction specific and ranges from -1.5 to -3.1 kA/m for the reversal

TABLE I. Magnetic fields H_{on} with initial perturbations of the magnetization of some electrodes during the magnetization reversal process from the parallel to the antiparallel configuration (P to AP) and vice versa (AP to P)

Junction	H_{on} (kA/m) P to AP	H_{on} (kA/m) AP to P
2	-3.1	0.5
4	-1.5	0.5
7	-1.5	0
8	-1.8	0
9	-2.6	0.5

from the parallel to the antiparallel configuration. During the reversal from the antiparallel to the parallel state, the perturbations take place at significantly lower magnetic fields between 0 and 0.5 kA/m. This asymmetry with respect to zero field originates from the ferromagnetic Néel coupling between the NiFe layer and the underlying antiferromagnet.¹⁵ Continuous films showed a Néel coupling field of $H_N = 1$ kA/m...2 kA/m, fitting well to the shifts observed for the patterned junctions. The reason for the large value of $H_{on} = -3.1$ kA/m in junction 2 could be resolved by MFM and arises from a domain wall in the center, which is extremely stable and prevents the junction from switching.

The investigation of rectangular MTJ's with 360 nm × 650 nm dimensions gave similar results as obtained for the larger junctions, except for a poorer quality of the MFM images due to the smaller magnetic moment and a tendency to a smaller Néel shift. This can be related to dipole coupling across the edges.⁵

C. Micromagnetic numerical simulations: Elliptical junctions

In the calculations for elliptical patterns, a common feature is found (Fig. 8). Elliptically patterned electrodes often show a high remanent magnetization [$M_X/M_S \approx 0.98$, Figs. 8(a) and 8(c)]. The shape, however, favors vortex formation due to minimalization of the stray field energy. Consequently, the magnetization reversal of elliptical junctions is often dominated by vortex nucleation and vortex motion with high saturation fields [Fig. 8(b) and 8(c)].

D. Domain observation by magnetic force microscopy: Elliptical junctions

The results of the simulations are experimentally proven by MFM investigations of the elliptically shaped MTJ's, where the complete layer stack including the antiferromagnet was patterned. In saturation or near saturation, the NiFe electrodes show a high magnetic contrast at their end points [Fig. 8(d)]. At $H = -1$ kA/m, the magnetization shows four opposite regions with bright or dark contrast, which is typical for a vortex state [Fig. 8(e)]. Thicker films with higher contrast show similar patterns more pronounced due to the larger stray fields [Fig. 8(f)].

IV. CONCLUSIONS

In summary, structural imperfections on the nanometer scale as imperfect corners and rough electrode boundaries

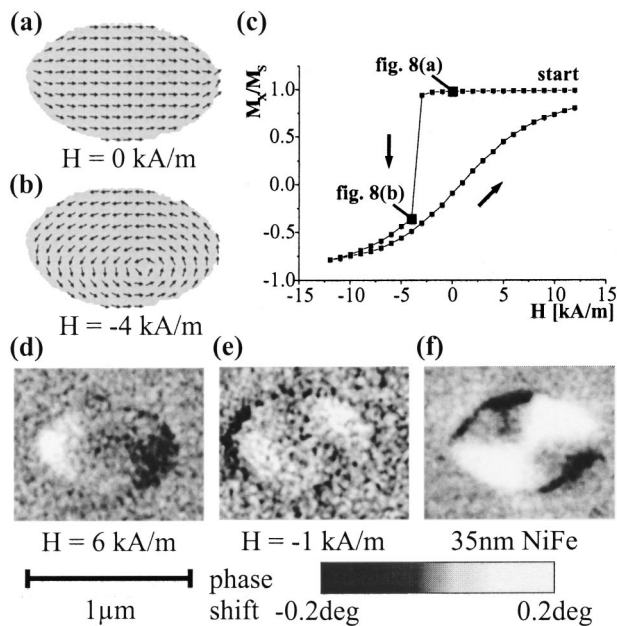


FIG. 8. Vortex nucleation in $500\text{ nm} \times 850\text{ nm}$ elliptical junctions. (a) and (b) Typical magnetization configurations. (c) Related magnetization curve. (d) to (f) MFM images of elliptically patterned magnetic tunnel junctions recorded at different stages of the minor loop. Additionally, an experimental MFM image of a vortex state in a 35 nm thick NiFe ellipse is shown.

cause junction specific magnetic switching behavior. Micro-magnetic numerical simulations with the real AFM shape show that these individual details significantly influence the nucleation, location, and mobility of domain walls. As a consequence, the overall switching fields strongly depend on boundary roughness. Initially, S-shaped magnetization is thus not sufficient for reliability and small switching fields in rectangular patterns. Boundary roughness determines the size

and stability of edge domains, which nucleate during the minor loops. Successive annihilation of them leads to steps in the magnetization curves.

Some features of the magnetic switching behavior are common, i.e., the nucleation of 180° walls in rectangular junctions with initially C-shaped magnetization and the nucleation of magnetization vortices in elliptical junctions. With regard to applications, an induced uniaxial anisotropy in the soft magnetic layer would help to reduce the influence of the boundary roughness.

ACKNOWLEDGMENTS

The authors thank J. Wecker, U. Klostermann, and G. Gieres (Siemens AG) for helpful discussions.

- ¹J. S. Moodera, L. R. Kinder, T. M. Wong, and R. Meservey, *Phys. Rev. Lett.* **74**, 3273 (1995).
- ²S. S. P. Parkin, K. P. Roche, M. G. Samant *et al.*, *J. Appl. Phys.* **85**, 5828 (1999).
- ³J. Schmalhorst, H. Brückl, G. Reiss, R. Kinder, G. Gieres, and J. Wecker, *Appl. Phys. Lett.* **77**, 3456 (2000).
- ⁴U. K. Klostermann, R. Kinder, G. Bayreuther, M. Rührig, G. Rupp, and J. Wecker, *J. Magn. Magn. Mater.* **240**, 305 (2002).
- ⁵H. Kubota, G. Reiss, H. Brückl, W. Schepper, and J. Wecker, *Jpn. J. Appl. Phys., Part 2* **41**, L180 (2002).
- ⁶Yu. Lu, R. A. Altman, A. Marley *et al.*, *Appl. Phys. Lett.* **70**, 2610 (1997).
- ⁷J. Schmalhorst, H. Brückl, G. Reiss, G. Gieres, and J. Wecker, *J. Appl. Phys.* **91**, 6617 (2002).
- ⁸Olympus ultra sharp etched silicon probes.
- ⁹M. Justus, H. Brückl, and G. Reiss, *J. Magn. Magn. Mater.* **240**, 212 (2002).
- ¹⁰OOMMF is available at <http://math.nist.gov/oommf> for public use.
- ¹¹J. Gadbois and J. -G. Zhu, *IEEE Trans. Magn.* **31**, 3802 (1995).
- ¹²Y. Zheng and J. -G. Zhu, *J. Appl. Phys.* **81**, 5471 (1997).
- ¹³U. Hartmann, *Phys. Lett. A* **137**, 475 (1989).
- ¹⁴H. Brückl, J. Schmalhorst, H. Boeve, G. Gieres, and J. Wecker, *J. Appl. Phys.* **91**, 7029 (2002).
- ¹⁵L. Néel, *C. R. Acad. Sci.* **255**, 1676 (1962).